PCP
PLANT & CELL PHYSIOLOGY

Inhibition of *CUTIN DEFICIENT 2* Causes Defects in Cuticle Function and Structure and Metabolite Changes in Tomato Fruit

Junji Kimbara[1,2], Miho Yoshida[1], Hirotaka Ito[1], Mamiko Kitagawa[1], Wataru Takada[1], Kayoko Hayashi[1], Yusuke Shibutani[1], Miyako Kusano[3], Yozo Okazaki[3], Ryo Nakabayashi[3], Tetsuya Mori[3], Kazuki Saito[3,4], Tohru Ariizumi[2] and Hiroshi Ezura[2,*]

[1]Research and Development Division, Kagome Co., Ltd., 17 Nishitomiyama, Nasushiobara, 329-2762 Japan
[2]Gene Research Center, University of Tsukuba, Tenno-dai 1-1-1, Tsukuba, 305-8572 Japan
[3]RIKEN Center for Sustainable Resource Science, 1-7-22 Suehiro-cho, Tsurumi-ku, Yokohama, Kanagawa, 230-0045 Japan
[4]Department of Molecular Biology and Biotechnology, Graduate School of Pharmaceutical Science, Chiba University, Chuo, Chiba, 260-8675 Japan
*Corresponding author: E-mail, ezura@gene.tsukuba.ac.jp; Fax, +81-29-853-7263
(Received June 1, 2013; Accepted July 3, 2013)

Regular Paper

Tomato (*Solanum lycopersicum*) fruit cuticle has been extensively studied due to its effect on the biochemical and physiological properties of the fruit. To date, several tomato mutants defective in proper cuticle formation have been identified. To gain insight into tomato cuticle formation, we investigated one such mutant, *sticky peel/light green* (*pe lg*). We verified the responsible gene by fine mapping and obtained the same conclusion as a previous report. To elucidate the pleiotropic effects of cuticle deficiency caused by the *cd2* mutation, *CD2* suppression lines were constructed. As found in the *pe lg* mutant, the suppression lines showed enhanced water permeability and aberrant leaf and fruit cuticles. Water use efficiency of the suppression line was lower than that of the wild type. However, photosynthetic ability was not affected in the suppression line. Since these phenotypes are related to altered deposition of wax and cutin, other lipidic metabolites might be changed, too. To confirm this hypothesis, we conducted metabolite profiling. The metabolite profiling revealed that not only lipid but also sugar, flavonoid and glycoalkaloid metabolites in fruit were changed in the *cd2* mutant. These results indicate that *CD2* is essential both for normal cutin and wax deposition and for proper accumulation of specific metabolites in tomato fruit.

Keywords: Cuticle • Fine mapping • Metabolomics • Tomato • Transpiration • Water permeability.

Abbreviations: DAG, diacylglycerol; GC-TOF-MS, gas chromatography coupled to time of flight mass spectrometry; LC-q-TOF-MS, liquid chromatography coupled to quadrupole time of flight mass spectrometry; lg, light green; PC, phosphatidylcholine; pe, sticky peel; PE, phosphatidylethanolamine; PG, phosphatidylglycerol; PI, phosphatidylinositol; PPFD, photosynthetic photon flux density; RT–PCR, reverse transcription–PCR; TB, toluidene blue; TEM, transmission electron microscopy.

Introduction

The plant's surface is exposed to many environmental challenges, including biotic and abiotic stresses. Due to their sessile nature, plants have evolved robust mechanisms to withstand these stresses. As the first barrier to stressors, the plant surface is covered with a cuticle layer consisting of several kinds of lipids (Riederer 2007), including wax and cutin. Cuticular wax is composed of very long-chain aliphatics (C >20), terpenoids, phenylpropanoids and flavonoids (Kunst and Samuels 2003). The wax composition and amount differ among species and even among tissues in an organism (Jetter et al. 2001, Samuels et al. 2008). Cuticular wax is thought to be involved in disease/pest resistance and minimizing transpiration (Vogg et al. 2004, Samuels et al. 2008, Leide et al. 2011). On the other hand, cutin is a polymer of oxygenated fatty acids that contains small amounts of glycerol and phenols (Heredia 2003, Pollard et al. 2008, Li and Beisson 2009). Cutin polymers are thought to confer resistance to mechanical damage, disease and pests, and to affect non-stomatal gas/water exchange (Pollard et al. 2008). Both wax and cutin are synthesized from fatty acids. The fatty acids are transported from the plastid to the endoplasmic reticulum, where they undergo modifications before being secreted from the cell (Jetter and Kunst 2008, Pollard et al. 2008). The synthesized components of wax and cutin, including the free fatty acids, alcohols, esters, aldehydes, alkanes and ketones from a few types of fatty acids (Kunst and Samuels 2003, Panikashvili et al. 2007), then traverse the thick cell wall of the epidermal cell, and are loaded onto the plant surface.

Plant Cell Physiol. 54(9): 1535–1548 (2013) doi:10.1093/pcp/pct100, available online at www.pcp.oxfordjournals.org

Mechanisms that regulate fatty acid flux in epidermal cells are not well understood (Samuels et al. 2008).

In Arabidopsis, several cuticle-related mutants have been identified and characterized to date. Common features of these mutants include changes in the amount and composition of cutin/wax (Schnurr et al. 2004, Li et al. 2007, Samuels et al. 2008), enhanced water permeability (Tanaka et al. 2004), postgenital organ fusion (Lolle et al. 1998) and altered disease resistance (Bessire et al. 2007, Curvers et al. 2010). Many of the genes affected in these mutants have been isolated (Yephremov and Schreiber 2005). Although a variety of compounds are known to constitute wax, its composition and the underlying biosynthetic pathways have only been partially elucidated. On the other hand, genes involved in cutin biosynthesis and polymerization appear to encode Cyt P450 (Xiao et al. 2004), transcription factors (Isaacson et al. 2009) and acyltransferases (Li et al. 2007, Yeats et al. 2012). Generally, cutin has fewer components than wax. However, the polymerization pattern of cutin is so complex that its structure remains to be clarified (Pollard et al. 2008).

Tomato fruit has a thick cuticle with a readily observable structure. Furthermore, the fruit cuticle of tomato, which grows in proportion to fruit development, is robust enough to be enzymatically isolated and physically analyzed (Bargel and Neinhuis 2005). Thus, tomato fruit is an excellent model for analyzing cuticle properties. To date, several mutants carrying defects in cuticle formation have been identified. Among the genes responsible for these mutants, *sitiens* (Curvers et al. 2010) and *Cwp1* (Hovav et al. 2007), involved in ABA production and of unknown function, respectively, affect cuticle formation indirectly. On the other hand, *CD1* (Yeats et al. 2012) and *CD2* (Isaacson et al. 2009) are directly involved in cuticle formation. The former encodes a cutin synthase, while the latter encodes a putative transcription factor. *CD2* was previously mapped and appeared to exert pleiotropic effects on plant development, such as increased water loss and susceptibility to microbial infection, most probably due to cutin deficiency. However, there was no clear correlation between the amount of cutin and water loss in the *cd2* mutant (Isaacson et al. 2009). The *cd2* mutation was reported to have pleiotropic effects in other species, too. The orthologs of *CD2* in Arabidopsis and rice play important roles in anthocyanin accumulation and leaf rolling, respectively, suggesting that the function of CD2 diversified during plant evolution, but that this gene is still important for normal plant development (Kubo et al. 1999, Kubo and Hayashi 2011, Zou et al. 2011).

We previously reported that the tomato variety KGM942, which carries both *sticky peel* (*pe*) and *light green* (*lg*) mutations, exhibits reduced cutin deposition and enhanced water permeability, and that *pe* and *lg* appear to be allelic (Kimbara et al. 2012). In this study, we performed map-based cloning to confirm the previous finding that *PE* and *LG* are monogenic and allelic to *CD2* (Nadakuduti et al. 2012). We also created *CD2* suppression lines and examined their morphological and biochemical features. We demonstrated that down-regulation of *CD2* resulted in enhanced water permeability in the leaf and fruit, consistent with a previous report (Kimbara et al. 2012). Dramatic alteration in cuticle components was observed in the *cd2* mutant (Isaacson et al. 2009, Nadakuduti et al. 2012), suggesting that other lipidic metabolites could be changed in the mutant. Thus, to explore the effect of the *cd2* mutation on fruit development, we performed metabolite profiling analyses, and found that the *cd2* mutation affects not only lipid, but also sugar, flavonoid and glycoalkaloid metabolites in fruit, whereas no other remarkable differences in other metabolites such as amino acids and other organic acids were found between the *cd2* mutant and wild-type varieties. In addition to reinforcing previously reported results (Isaacson et al. 2009, Nadakuduti et al. 2012), our findings demonstrate that mutation of *CD2* causes partial metabolite changes in tomato fruit.

Results

Fine mapping of *PE LG* revealed a frameshift mutation in *CD2*

In a classic report, the *pe* and *lg* mutations were suggested to segregate (Butler 1952) and *PE* was proposed to be located on the long arm of chromosome 1 (Kerr 1982). In contrast, our previous results suggested that *pe* and *lg* of KGM942 are most probably allelic (Kimbara et al. 2012). To confirm our previous findings, we generated an F_2 mapping population derived from a cross between KGM942 (*pe*/*pe*, *lg*/*lg*) and the wild-type variety Rejina (*PE*/*PE*, *LG*/*LG*). Among the 334 F_2 plants produced, 82 had a phenotype typical of the *pe lg* mutant, i.e. light green leaf color and thin fruit peel. We tested three markers located on the long arm of chromosome 1 using the F_2 population, which carried the *pe lg* mutation (**Supplementary Table S1**). Recombination rates of C2_At2g38730 (92.5 cM), C2_At3g04710 (95 cM) and SSR222 (97.5 cM) were 0.130, 0.154 and 0.154, respectively. Thus, we concluded that *PE LG* could be located on the centromeric side of C2_At2g38730 (92.5 cM).

For fine mapping of *PE LG*, we created an F_2 population derived from a cross between KGM942 and IL1-2, which carries the chromosomal segment of *Solanum pennellii* from the centromeric region to TG295 (92.7 cM) of chromosome 1. Among 1,600 F_2 plants, *pe* was certainly linked with *lg*, and 336 were selected based on the *pe lg* phenotype as described above. We tested 12 polymorphic markers between KGM942 and IL1-2 from 55 to 73 cM on chromosome 1 for all 336 individuals showing the *pe lg* phenotype (**Supplementary Table S2**). The solcap_snp_sl_100409, Solyc01g091500_1, C2_At3g61140 and Solyc01g091720_1 markers were perfectly linked with the *pe lg* phenotype. The narrowed down region in which these markers were located spanned 462.3 kb, and was mapped to the long arm of chromosome 1 (**Supplementary Fig. S1**). Based on the Solanaceae consortium database (SGN), this region contains 56 predicted open reading frames (ORFs), one of which is *CD2*, which is known to be involved in proper

cuticle formation (Isaacson et al. 2009, Nadakuduti et al. 2012). Given that *cd2* has a cutin deficiency and altered water permeability, a phenotype that resembles that of KGM942 (*pe lg*), and that *PE* and *LG* may be allelic (Kimbara et al. 2012), we hypothesized that *PE* and *LG* are allelic, and that *CD2* is the gene altered in the *pe lg* mutation. To test these hypotheses, we determined the genomic sequence of *CD2* in Rejina and KGM942 and found that there was a 1 bp insertion in the eighth exon only of KGM942 (**Supplementary Table S1**). This insertion causes a frameshift mutation that truncates the latter part of CD2, resulting in the production of a stop codon at the 662nd amino acid. Our result agreed with the previous finding that the *pe* phenotype was caused by the frameshift mutation of *CD2* (Nadakuduti et al. 2012).

If both the *pe* and *lg* phenotypes are indeed caused by a single mutation in *CD2*, we expected *CD2* to be expressed in both the leaf and fruit, because the *pe lg* mutations caused morphological alterations in the vegetative and reproductive tissues. As we expected, *CD2* mRNA was present in all tissues tested (**Fig. 1**).

Together, these results suggest that the 1 bp insertion of *CD2* is probably the cause of the *pe lg* phenotype.

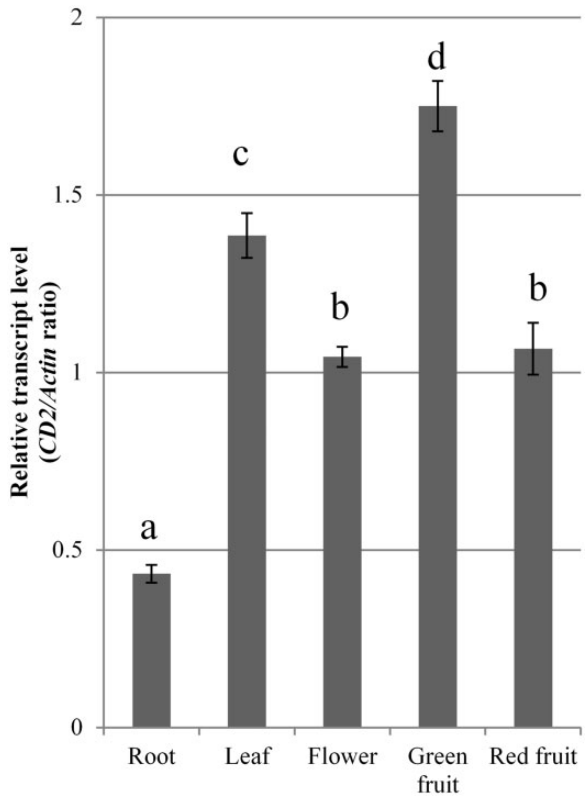

Fig. 1 *CD2* expression in various tissues. cDNAs synthesized from total RNA were amplified using primer pairs specific for *Actin* and *CD2*. *CD2* expression is presented relative to the amount of *Actin* RNA. Vertical bars indicate the SD ($n = 3$). Columns with different letters indicate significant differences (ANOVA and Tukey's test; $P < 0.05$).

Leaf cuticle was decreased and water permeability was enhanced in the *CD2* suppression lines

To demonstrate that both the pale leaf color and the cutin deficiency in fruit and leaves were due to disruption of CD2, *CD2* suppression lines were created using an antisense strategy. In total, 18 transgenic lines were created and the *CD2* expression levels of transgenic plants in the T_0 generation were determined. As shown in **Fig. 2a**, *CD2* expression was greatly suppressed in transgenic lines AS12, AS16, AS17 and AS38 (**Fig. 2a**). Among these, three transgenic lines, AS16, AS17 and AS38, were selected for further analysis. The obtained *CD2* suppression lines grew normally and, although several cuticle-related mutants are known to have reduced fertility (Aarts et al. 1995, Millar et al. 1999, Leide et al. 2011), their fertility was not affected.

The young leaves of these suppression lines were pale green, consistent with the fact that KGM942 has pale green leaves (Kimbara et al. 2012; **Fig. 2b**). To explore the molecular basis of this phenotype, we determined the Chl content of leaves derived from these plants. Whereas no significant difference in Chl *a* content was found between the suppression lines and the wild type, the Chl *b* content was significantly greater in the suppression lines than in the wild type (**Supplementary Fig. S2**). These results are consistent with a previous report that *pe lg* mutations somewhat influence the Chl *b* content (Kimbara et al. 2012). In contrast, no remarkable difference in leaf color was found in the old leaves of the wild type and the suppression lines (**Fig. 2c**), suggesting that the leaf color phenotype was specific to the early stages of plant development.

Since *cd2* and *pe lg* mutations are known to influence cuticle deposition, we next examined the leaf cuticle ultrastructure using transmission electron microscopy (TEM) (**Fig. 3**). On the adaxial side, the innermost dense layer, the 'cuticle layer' in the suppression lines, was thinner than that in the wild type, though the translucent layer, the 'cuticle proper' in the suppression lines, was not affected (Kosma et al. 2009) (**Fig. 3a–d**). In contrast, no remarkable difference was found in the structure and electron density of the cuticle proper and the cuticle layer between the suppression lines and wild type on the abaxial side (**Fig. 3e–h**).

To investigate whether a cuticle deficiency in the *CD2* suppression lines influences water permeability, we measured the transpiration rate and performed toluidine blue (TB) staining. Prior to measuring transpiration rates, the leaves were treated with ABA to induce stomatal closure, and the rate of water loss was compared between the wild type and the suppression lines. Transpiration rates in the suppression lines were significantly higher than in the wild type, indicating that water loss from leaves was enhanced in the suppression lines (**Fig. 4a**). In addition, the leaves of the suppression lines stained relatively strongly with TB, whereas those of the wild type did not stain at all (**Fig. 4b**), indicating that externally applied water penetrated leaf tissues more efficiently in the suppression lines. Therefore, water permeability in the leaf cuticle was enhanced in the suppression lines. These results are consistent with those

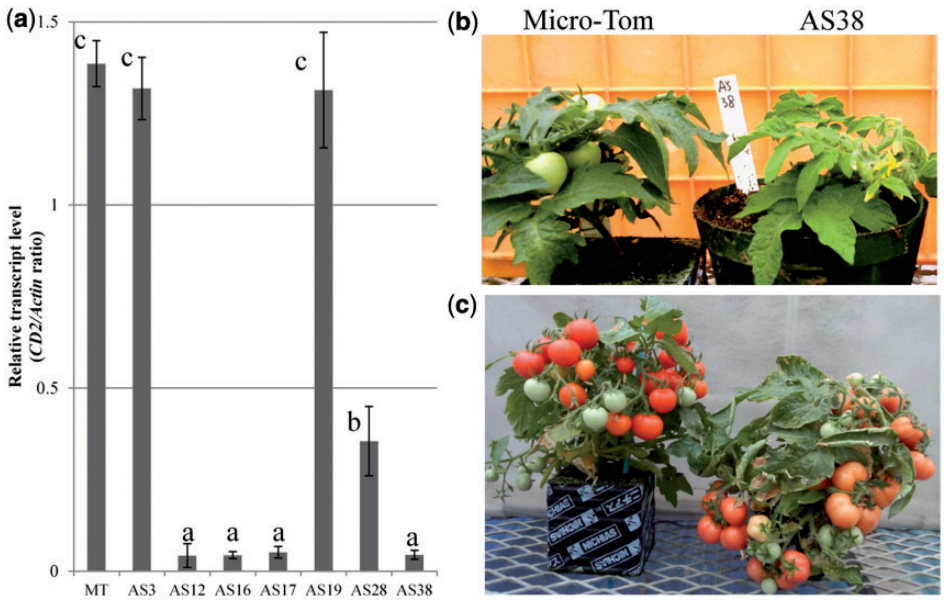

Fig. 2 Construction of the *CD2* suppression lines. (a) CD2 expression in the leaves of the CD2 suppression lines. cDNAs synthesized from total RNA were amplified using primer pairs specific for *Actin* and the 5′-untranslated region (UTR) of *CD2*. *CD2* expression is presented relative to the amount of *Actin* RNA. Vertical bars indicate the SD ($n = 3$). Columns with different letters indicate significant differences (ANOVA and Tukey's test; $P < 0.05$). (b) Seedling stage and (c) mature stage of Micro-Tom (left) and the suppression line AS38 (right). Scale bars indicate 2 cm (b) and 5 cm (c).

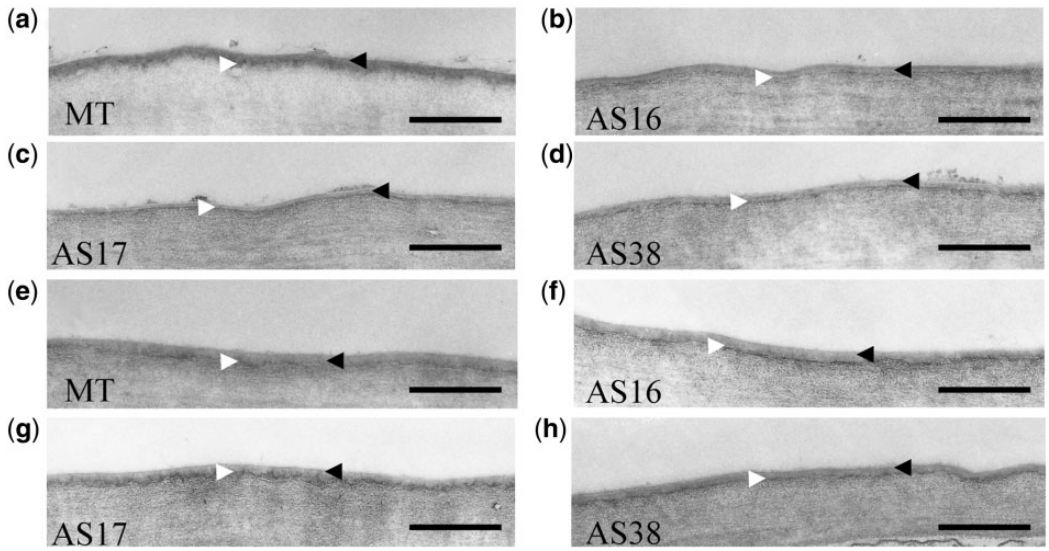

Fig. 3 Cross-sections through the leaves of Micro-Tom and the *CD2* suppression lines. TEM images of the adaxial (a–d) and abaxial (e–h) leaf surfaces. Micro-Tom (MT; a, e) and the suppression lines AS16 (b, f), AS17 (c, g) and AS38 (d, h). The cuticle proper is indicated by black arrowheads and the cuticle layer by white arrowheads (e–l). Scale bars indicate 500 nm.

of previous reports and reinforce the hypothesis that *CD2* suppression promotes water permeability (Kimbara et al. 2012, Nadakuduti et al. 2012).

Water use efficiency is decreased in the suppression lines

The enhancement of water permeability in the suppression lines may affect the rates of photosynthesis and gas exchange. Thus, the photosynthetic ability and water use efficiency were analyzed using the LI-6400XT Portable Photosynthesis and Fluorescence System. Interestingly, the photosynthetic rate at a photosynthetic photon flux density (PPFD) of 0–1,500 μmol m^{-2} s^{-1} was not significantly different between the suppression line and the wild type (**Fig. 5a**), indicating that photosynthetic ability was not affected in the suppression line. However, the transpiration rate of the suppression line was

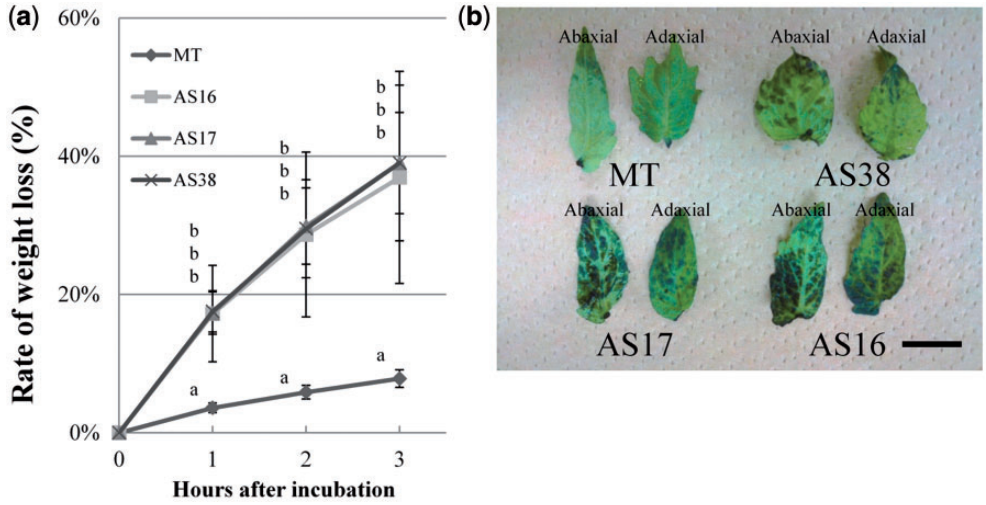

Fig. 4 Water permeability of the leaves. (a) Rate of dehydration measured as fresh weight loss of the wild-type variety Micro-Tom (MT) and three *CD2* suppression lines (AS16, AS17 and AS38). Vertical bars indicate the SD ($n = 5$). Columns with different letters indicate significant differences (ANOVA and Tukey's test; $P < 0.05$). (b) TB staining pattern of the wild-type variety Micro-Tom (MT) and the suppression lines (AS16, AS17 and AS38). Abaxial (left) and adaxial (right) sides of the leaf are shown for each line. Scale bars indicate 1 cm.

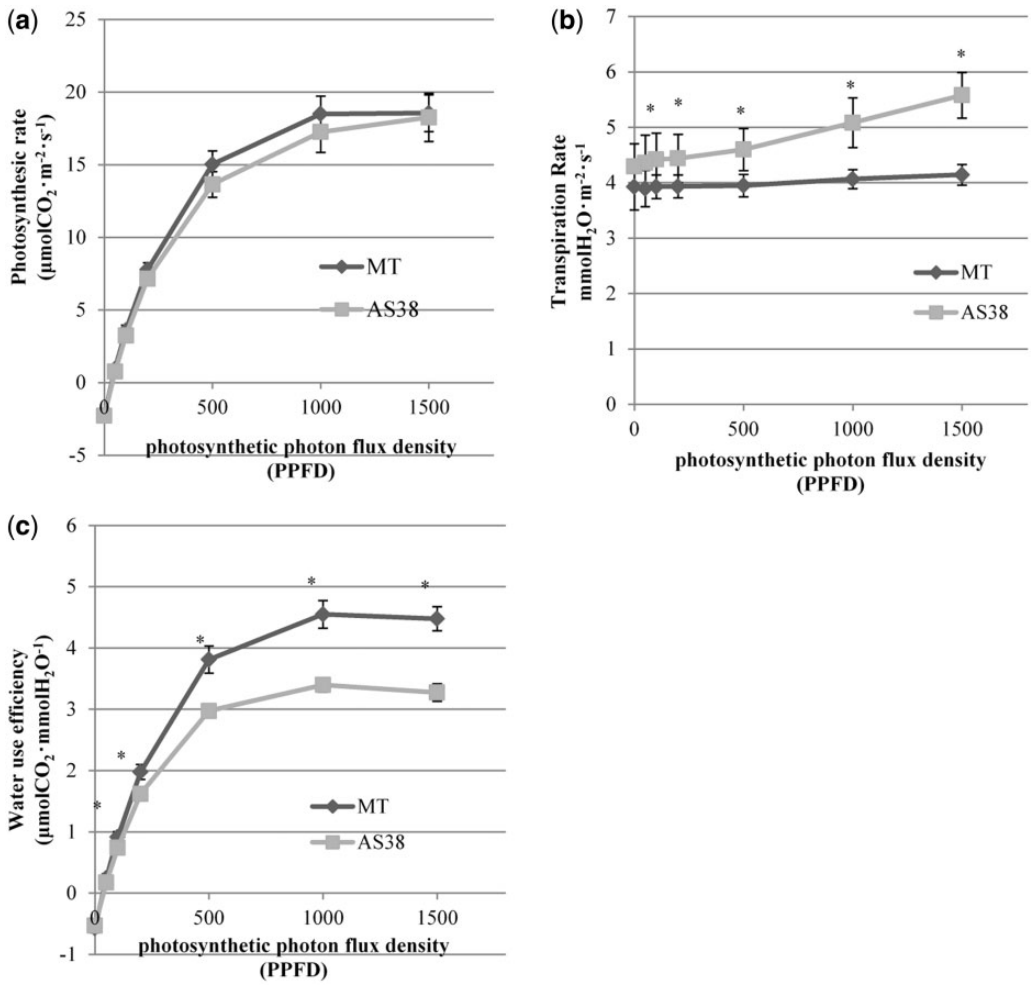

Fig. 5 Photosynthetic ability and water use efficiency. (a) Photosynthetic rate. (b) Transpiration rate. (c) Water use efficiency. Micro-Tom was used as the wild-type variety, and AS38 as the suppression line. Vertical bars indicate the SD ($n = 5$). Asterisks indicate significant differences (*t*-test; $P < 0.05$).

significantly higher at a PPFD of 100–1,500 (**Fig. 5b**). Therefore, water use efficiency of the suppression lines in the same PPFD range was significantly decreased compared with that of the wild type (**Fig. 5c**). This difference is not due to differences in stomatal density between the wild type and suppression line, because the stomatal density of the suppression line was significantly lower than that of the wild type (**Supplementary Fig. S3**).

The *CD2* suppression lines have thinner fruit cuticles and enhanced water permeability in the fruit

The fruit of the suppression lines was more glossy and paler red (pink) than that of the wild type (**Fig. 6a**). Moreover, the fruit cuticle was thinner in the suppression lines (**Fig. 6b–e**). The glossiness and thin cuticle of the suppression lines were consistent with the phenotypes of the *cd2* and *pe lg* mutants (Isaacson et al. 2009, Kimbara et al. 2012, Nadakuduti et al. 2012). However, the pale red color of the *CD2* suppression lines was unexpected, since neither *cd2* nor *pe lg* had altered fruit color. It is possible that the intensity of fruit color is negatively correlated with the degree of *CD2* inhibition.

In the leaf tissue, the cuticle deficiency caused by *CD2* suppression resulted in enhanced water permeability. Thus, we evaluated the water permeability of the fruit in the suppression lines. Generally, the tomato fruit cuticle is much thicker than that of the leaf, and resists water loss through transpiration. In our results, the fruit cuticle of the suppression lines was actually thinner than that of the wild type (**Fig. 6b–e**). However, the transpiration rate of AS17 was not significantly different from that of the wild type throughout the experiment (**Fig. 7a**). Moreover, another suppression line, AS16, did not show a significant increase in transpiration rate at the end of the experiment (**Fig. 7a**). These results were different from those for leaves in that the corresponding suppression lines showed significantly higher water permeability than Micro-Tom.

Metabolite profiling analyses revealed altered composition of lipids, flavonoids, glycoalkaloids and sugars in the *cd2* mutant

The composition and amount of lipidic cuticle components is known to differ in the *cd2* mutant compared with the wild type (Isaacson et al. 2009, Kimbara et al. 2012, Nadakuduti et al. 2012) in both vegetative and reproductive tissues (Nadakuduti et al. 2012). Therefore, the levels of metabolites of an entire tissue type might be changed in the *cd2* mutant. Thus, we subjected the pericarps of mature red fruits of the *cd2* mutant (KGM942) and the three wild-type varieties, Ec-1, RC17 and K091, to metabolite profiling analyses of lipids, flavonoids, glycoalkaloids and other primary metabolites using gas chromatography coupled to time of flight mass spectrometry (GC-TOF-MS) and liquid chromatography coupled to quadrupole time of flight mass spectrometry (LC-q-TOF-MS). The physiological properties of the three wild-type varieties used here were previously analyzed (Kimbara et al. 2012).

We performed principal component analysis (PCA) to visualize the distribution of samples in the first two components (**Supplementary Fig. S4**). Samples of the *cd2* mutant and those of the three wild-type varieties were separated along the first principal component ($R^2 = 0.244$). Along the second principal component ($R^2 = 0.127$), samples were grouped together with respect to the variety-dependent differences of the wild type. These results indicate that the mutation also influenced the metabolite composition of the *cd2* mutant. The effect was large enough to distinguish the mutant from the wild-type varieties, and each wild-type variety had visual phenotypic differences in fruit and different genetic backgrounds (Kimbara et al. 2012).

Among the lipid-related metabolites, the contents of all annotated fatty acids and acyl glycerols except for diacylglycerol (DAG) 34:3 and DAG 36:5 were not significantly different among the *cd2* mutant and the three wild-type varieties (**Table 1**). However, all glycolipids other than β-sitosteryl (6′-*O*-linolenoyl) glucoside, β-sitosteryl (6′-*O*-palmitoyl) glucoside

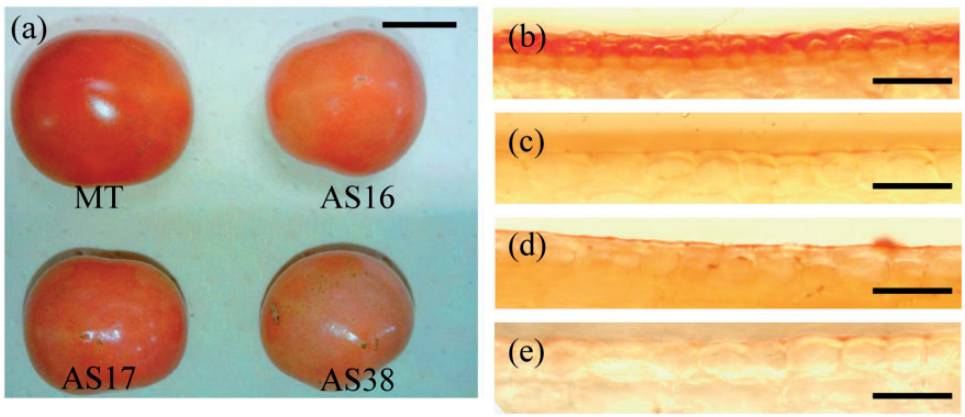

Fig. 6 The fruit of Micro-Tom and the *CD2* suppression lines. (a) Ripe fruit of Micro-Tom (MT) and the *CD2* suppression lines (AS16, AS17 and AS38). Microscopy images of epidermal sections of MT fruit (b) and the suppression lines (c–e). Scale bars indicate 1 cm (a) and 50 μm (b–e).

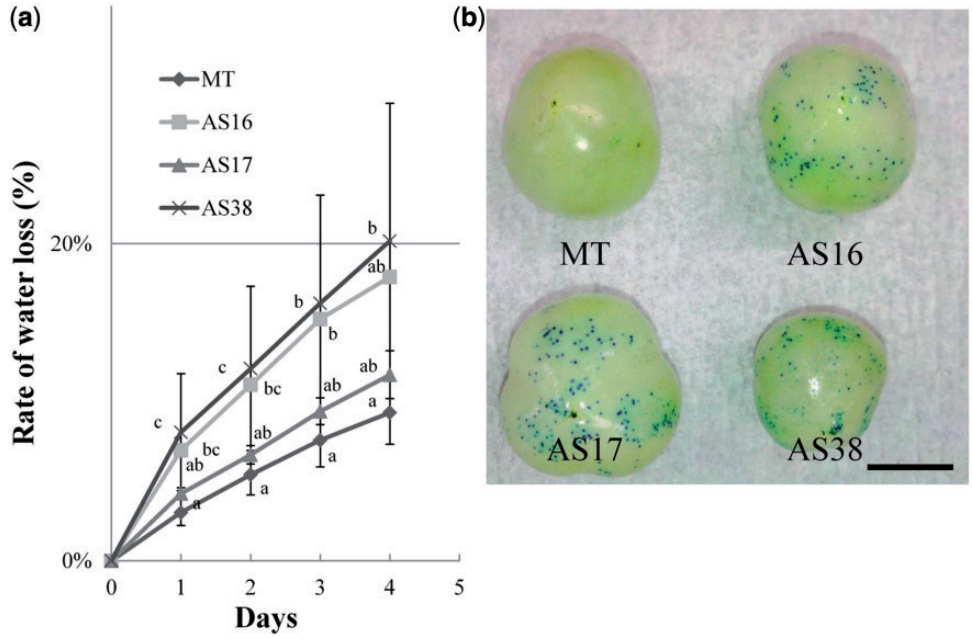

Fig. 7 Water permeability of the fruit of Micro-Tom (MT) and the *CD2* suppression lines. (a) Fruit transpiration rate of the wild-type variety MT and the three suppression lines (AS16, AS17 and AS38). Vertical bars indicate the SD ($n = 5$). Columns with different letters indicate significant differences (ANOVA and Tukey's test; $P < 0.05$). (b) Fruit TB staining pattern of the wild-type variety MT and the suppression lines (AS16, AS17 and AS38). Scale bar indicates 1 cm.

and sitosteryl glucoside were significantly higher in the *cd2* mutant (**Table 1**). Similarly, lyso phosphatidylcholine (PC) 16:0, phosphatidylethanolamine (PE) 34:2, PE 36:2, phosphatidylglycerol (PG) 34:2, phosphatidylinositol (PI) 34:2 and PI 34:3 in the phospholipid category were more abundant in the *cd2* mutant.

Next, we investigated changes of the levels of flavonoids and glycoalkaloids. Flavonoids and alkaloids were also more abundant in the *cd2* mutant (**Table 2**). Notably, significant increases in flavonoid glycosides and glycoalkaloids such as kaempferol-3-*O*-rutinoside, naringenin dihexose, quercetin-dihexose-deoxyhexose, rutin, tomatine and its derivatives and escleoside and its derivatives strongly suggest that sugar metabolism is most probaby altered in the *cd2* mutant. Next, we investigated changes of the levels of sugar and its derivatives, such as sugar acid and sugar alcohol. The levels of *N*-acetylglucosamine, arabinose and xylose were abundant in the *cd2* mutant (**Table 3**). However, glucose, fructose and sucrose, which are major sugar components of tomato fruit, were not significantly different between the *cd2* mutant and wild-type varieties (**Table 3**). On the other hand, we detected several significant differences in the abundance of sugar acids and sugar alcohols, including galacturonic acid, glucuronic acid-e-lactone, saccharic acid and galactinol, and glyceric acid and myo-inositol between the *cd2* mutant and the wild-type varieties (**Table 3**). Although we cannot conclude whether these metabolic changes are the direct effect of the *cd2* mutation, this result may support the hypothesis that sugar metabolism is altered in the mutant.

We annotated two carotenoids: β-carotene and lycopene (**Table 4**). The lycopene content in the *cd2* mutant was significantly higher than in the wild-type varieties. Although we did not analyze the carotenoid contents of the fruits in the suppression lines, this result implies that the carotenoid composition was also affected in the *cd2* mutant. As described above, the fruit color of the *pe lg* mutant differed from that of the suppression lines. This might be due to differences in the extent of CD2 inhibition between the *pe lg* mutant and the suppression lines. Alternatively, this may be caused by differences in the genetic backgrounds of the tested lines. Thus, future studies should quantify fruit carotenoid accumulation in the *cd2* mutant.

Other major fruit components, such as amino acids and other organic acids, did not differ significantly between the *cd2* mutant and wild-type varieties (**Supplementary Tables S3**, **S4**). Thus, changes in sugar and lipid metabolism are prominent in the *cd2* mutant.

Discussion

The pleiotropic effects of *CD2* suppression on vegetative and reproductive tissues

In this study, we mapped the gene underlying the *pe lg* phenotype. The mapped region fell within a 462.3 kb region of chromosome 1 (**Supplementary Fig. S1**). Since this region contains *CD2*, which is known to be involved in cuticle formation (Isaacson et al. 2009), we determined the sequence of the coding region of *CD2*. As others have reported (Nadakuduti et al. 2012), we identified a 1 bp insertion in the coding region of *CD2* in the *pe lg* mutant. Then, we generated *CD2*

Table 1 Lipid composition in tomato fruits of the mutant and three cultivars

Metabolite	Method	Arbitrary unit (AU) ±SD			
		Ec-1	RC17	K091	KGM942
Fatty acids					
Linoleic acid	GC	31.21 ± 0.78a	30.74 ± 0.89a	30.26 ± 0.47a	30.95 ± 0.50a
Palmitic acid	GC	25.30 ± 0.95a	24.94 ± 1.13a	24.39 ± 0.64a	25.10 ± 0.66a
Acyl glycerols					
DAG 34:2	LC1	−2.38 ± 0.14b	−2.66 ± 0.14a	−2.39 ± 0.19b	−2.25 ± 0.32b
DAG 34:3	LC1	−4.29 ± 0.16b	−4.08 ± 0.24b	−4.61 ± 0.16a	−3.70 ± 0.40c
DAG 36:4	LC1	−3.71 ± 0.17b	−4.25 ± 0.08a	−3.92 ± 0.14b	−3.92 ± 0.42b
DAG 36:5	LC1	−4.95 ± 0.10a	−5.01 ± 0.14a	−5.22 ± 0.25a	−4.61 ± 0.41b
TAG 50:2	LC1	−5.06 ± 0.27b	−4.98 ± 0.28b	−5.83 ± 0.45a	−5.25 ± 0.86ab
TAG 52:3	LC1	−6.84 ± 0.36a	−7.52 ± 0.52a	−7.26 ± 0.45a	−7.20 ± 1.24a
TAG 52:4	LC1	−3.11 ± 0.33a	−3.51 ± 0.32a	−3.34 ± 0.59a	−3.76 ± 0.97a
TAG 52:5	LC1	−2.90 ± 0.26ab	−2.63 ± 0.33b	−3.26 ± 0.77ab	−3.63 ± 0.86a
TAG 54:6	LC1	−3.50 ± 0.38b	−4.38 ± 0.43ab	−3.61 ± 0.63b	−4.52 ± 1.18a
TAG 54:7	LC1	−2.53 ± 0.22b	−2.80 ± 0.37b	−2.92 ± 0.73ab	−3.65 ± 0.96a
TAG 54:8	LC1	−3.10 ± 0.23b	−3.12 ± 0.32b	−3.61 ± 0.77ab	−4.05 ± 0.90a
Glycolipids					
Campesteryl (6′-*O*-palmitoyl) glucoside	LC1	−4.14 ± 0.12a	−3.36 ± 0.13c	−3.94 ± 0.15b	−3.18 ± 0.11d
MGDG 34:3	LC1	−5.28 ± 0.14a	−4.09 ± 0.32b	−3.94 ± 0.31b	−3.48 ± 0.24c
MGDG 36:4	LC1	−2.60 ± 0.21b	−3.74 ± 0.42a	−3.55 ± 0.35a	−1.71 ± 0.58c
MGDG 36:5	LC1	−2.65 ± 0.20b	−3.26 ± 0.39a	−3.32 ± 0.37a	−1.35 ± 0.42c
MGDG 36:6	LC1	−1.80 ± 0.14a	−0.94 ± 0.28b	−0.48 ± 0.20c	0.27 ± 0.15d
DGDG 34:1	LC1	−7.03 ± 0.29b	−7.85 ± 0.41a	−6.51 ± 0.36c	−5.75 ± 0.58d
DGDG 34:2	LC1	−2.97 ± 0.15c	−3.80 ± 0.34a	−3.44 ± 0.24b	−2.51 ± 0.37d
DGDG 34:3	LC1	−4.06 ± 0.13a	−3.12 ± 0.27b	−2.61 ± 0.26c	−1.90 ± 0.15d
DGDG 36:3	LC1	−6.15 ± 0.09a	−5.79 ± 0.14b	−5.43 ± 0.28c	−4.11 ± 0.14d
DGDG 36:4	LC1	−5.09 ± 0.21b	−6.12 ± 0.31a	−5.69 ± 0.22a	−3.98 ± 0.64c
DGDG 36:5	LC1	−4.64 ± 0.24b	−5.78 ± 0.43a	−5.31 ± 0.43a	−3.14 ± 0.53c
DGDG 36:6	LC1	−3.65 ± 0.14a	−3.16 ± 0.23b	−2.53 ± 0.19c	−1.19 ± 0.14d
β-Sitosteryl (6′-*O*-linolenoyl) glucoside	LC1	−4.64 ± 0.24a	−4.79 ± 0.30a	−3.94 ± 0.21b	−3.90 ± 0.21b
β-Sitosteryl (6′-*O*-linoleoyl) glucoside	LC1	−5.95 ± 0.15b	−6.12 ± 0.20ab	−6.18 ± 0.22a	−4.77 ± 0.28c
β-Sitosteryl (6′-*O*-palmitoyl) glucoside	LC1	−1.98 ± 0.16a	−2.03 ± 0.25a	−1.45 ± 0.13b	−1.30 ± 0.15b
Sitosteryl glucoside	LC1	−4.63 ± 0.20a	−4.79 ± 0.35a	−4.20 ± 0.13b	−4.23 ± 0.31b
SQDG 34:3	LC1	−5.65 ± 0.19a	−5.20 ± 0.21b	−5.20 ± 0.16b	−4.34 ± 0.15c
Phospholipids					
lysoPC 16:0	LC1	−5.33 ± 0.29a	−5.38 ± 0.19a	−4.98 ± 0.21b	−4.34 ± 0.20c
PC 34:1	LC1	−2.08 ± 0.33b	−2.28 ± 0.53ab	−2.57 ± 0.24a	−1.97 ± 0.40b
PC 34:2	LC1	1.86 ± 0.14a	1.93 ± 0.10a	1.96 ± 0.19a	2.02 ± 0.09a
PC 34:3	LC1	−0.24 ± 0.15a	0.59 ± 0.21b	−0.21 ± 0.18a	0.39 ± 0.11b
PC 34:4	LC1	−6.42 ± 0.16a	−5.73 ± 0.18b	−5.16 ± 0.38c	−5.14 ± 0.33c
PC 36:2	LC1	−1.78 ± 0.18b	−1.99 ± 0.10a	−2.12 ± 0.17a	−1.72 ± 0.14b
PC 36:3	LC1	−2.24 ± 0.35a	−2.15 ± 0.42a	−1.92 ± 0.17ab	−1.65 ± 0.44b
PC 36:4	LC1	1.26 ± 0.18a	1.34 ± 0.09ab	1.47 ± 0.17b	1.43 ± 0.12ab
PC 36:5	LC1	−0.30 ± 0.14a	0.46 ± 0.19c	−0.05 ± 0.16b	0.31 ± 0.09c
PC 36:6	LC1	−3.92 ± 0.21a	−2.51 ± 0.37c	−3.31 ± 0.20b	−2.61 ± 0.11c
PE 34:2	LC1	−0.80 ± 0.10a	−0.63 ± 0.09b	−0.39 ± 0.14c	−0.20 ± 0.10d
PE 34:3	LC1	−3.19 ± 0.16a	−2.51 ± 0.23b	−3.16 ± 0.16a	−2.41 ± 0.13b

(continued)

Table 1 Continued

Metabolite	Method	Arbitrary unit (AU) ±SD			
		Ec-1	RC17	K091	KGM942
PE 36:2	LC1	−5.02 ± 0.16a	−4.96 ± 0.09a	−4.94 ± 0.15a	−4.52 ± 0.13b
PE 36:3	LC1	−6.30 ± 0.35a	−6.22 ± 0.26a	−5.16 ± 0.25b	−5.41 ± 0.52b
PE 36:4	LC1	−1.89 ± 0.14a	−1.52 ± 0.08b	−1.32 ± 0.16c	−1.22 ± 0.15c
PE 36:5	LC1	−3.94 ± 0.14a	−3.20 ± 0.20b	−3.76 ± 0.18a	−3.29 ± 0.19b
PG 34:2	LC1	−6.26 ± 0.23a	−6.48 ± 0.19a	−6.30 ± 0.20a	−5.47 ± 0.37b
PG 34:3	LC1	−7.39 ± 0.23a	−6.65 ± 0.34b	−5.74 ± 0.11c	−5.46 ± 0.30c
PI 34:2	LC1	−3.46 ± 0.15a	−3.40 ± 0.09a	−3.23 ± 0.12b	−3.00 ± 0.18c
PI 34:3	LC1	−5.18 ± 0.21a	−4.76 ± 0.24b	−5.22 ± 0.14a	−4.23 ± 0.15c

All data were log2 transformed. Metabolites in bold are significantly different between the mutant variety KGM942 and the wild-type varieties, Ec-1, RC17 and K091. All comparisons among means (ANOVA and Tukey's test; $P < 0.05$, sample size $n = 10$) were used to determine differences between the cultivars.
Different lower case letters in a column indicate significant differences.
DAG, diacylglycerol; DGDG, digalactosyl diacyl glycerol; MGDG, monogalactosyl diacyl glycerol; PC, phosphatidylcholine; PE, phosphatidylethanolamine; PG, phosphatidylglycerol; PI, phosphatidylinositol. TAG, triacylglycerol.

Table 2 Flavonoid and glycoalkaloid composition in tomato fruits of the mutant and three cultivars

Metabolite	Method	Arbitrary unit (AU) ±SD			
		Ec-1	RC17	K091	KGM942
Flavonoids					
Kaempferol-3-*O*-rutinoside	LC2	−5.30 ± 0.29a	−4.05 ± 0.80b	−4.01 ± 0.72b	−1.36 ± 0.31c
Kaempferol-hexose-deoxyhexose-pentose	LC2	−4.46 ± 0.82a	−4.20 ± 0.68a	−3.89 ± 0.57a	−4.14 ± 0.26a
Naringenin or naringenin chalcone	LC2	−1.45 ± 1.03b	−0.22 ± 1.77bc	−5.43 ± 0.10a	0.86 ± 0.53c
Naringenin dihexose	LC2	−4.96 ± 0.67a	−3.82 ± 0.66b	−5.44 ± 0.10a	−1.50 ± 0.30c
Quercetin-dihexose-deoxyhexose	LC2	−5.23 ± 0.32a	−4.30 ± 0.95b	−2.79 ± 0.76c	−0.76 ± 0.42d
Quercetin-hexose-deoxyhexose-pentose	LC2	−1.23 ± 0.83a	−0.93 ± 0.81a	−1.34 ± 0.67a	−1.22 ± 0.22A
Rutin	LC2	−1.24 ± 1.01a	0.59 ± 0.77b	−0.12 ± 0.72b	2.09 ± 0.15C
Alkaloids					
Acetoxyesculeoside B	LC2	−5.58 ± 0.58a	−4.52 ± 0.51b	−5.29 ± 0.40a	−3.92 ± 0.28c
Acetoxy-hydroxytomatine isomer #1	LC2	−6.31 ± 0.03a	−6.22 ± 0.14a	−6.29 ± 0.03a	−4.61 ± 0.36b
Acetoxytomatine 1	LC2	−6.31 ± 0.03a	−6.15 ± 0.19a	−6.29 ± 0.03a	−5.51 ± 0.33b
Acetoxytomatine 2	LC2	−6.26 ± 0.11a	−5.30 ± 0.65b	−5.87 ± 0.44ab	−5.44 ± 0.40b
α-Tomatine, α -tomatine isomer	LC2	−6.31 ± 0.03a	−5.65 ± 0.63b	−6.29 ± 0.03a	−3.09 ± 0.50c
Dehydrolycoperoside G/F ordehydroesculeoside A (isomer #1,#2,#3)	LC2	−5.87 ± 0.43a	−4.91 ± 0.50b	−5.00 ± 0.35b	−3.89 ± 0.28c
Dehydrotomatidine (tomatidenol) 1	LC2	−6.31 ± 0.03a	−6.29 ± 0.04a	−6.29 ± 0.03a	−5.15 ± 0.42b
Dehydrotomatidine (tyomatidenol) 2	LC2	−6.30 ± 0.03a	−6.24 ± 0.16a	−6.29 ± 0.03a	−6.27 ± 0.05a
Dehydrotomatine isomer #1,#2,#3,#4,#5,#6	LC2	−6.31 ± 0.03a	−6.29 ± 0.04a	−6.29 ± 0.03a	−5.84 ± 0.43b
Esculeoside B isomer 1,2,3,4	LC2	−6.31 ± 0.03a	−6.29 ± 0.04a	−6.29 ± 0.03a	−5.37 ± 0.94b
Hydroxytomatine isomer #1,#2,#3,#4,#5,#6,#7	LC2	−5.53 ± 0.51a	−4.44 ± 0.40c	−4.94 ± 0.25b	−4.25 ± 0.28c
Lycoperoside G/F oresculeoside A + hexose-pentose	LC2	−6.23 ± 0.18a	−5.73 ± 0.43b	−6.06 ± 0.31ab	−5.08 ± 0.32c
Lycoperoside G/F or esculeoside A + hexose (isomer #1,#2,#3,#4,#5,#6)	LC2	−5.73 ± 0.73a	−4.73 ± 0.59b	−5.28 ± 0.45ab	−5.48 ± 0.23a
Tomatidine, tomatidine isomer	LC2	−6.28 ± 0.10a	−4.50 ± 0.82b	−6.29 ± 0.03a	−2.20 ± 0.42c
UGA 8	LC2	−6.31 ± 0.03a	−5.93 ± 0.56b	−6.28 ± 0.03ab	−6.17 ± 0.22ab
UGA 10	LC2	−6.31 ± 0.03a	−6.26 ± 0.08a	−6.27 ± 0.05a	−5.19 ± 0.71b

All data were log2 transformed. Metabolites in bold are significantly different between the mutant variety KGM942 and the wild-type varieties, Ec-1, RC17 and K091. All comparisons among means (ANOVA and Tukey's test; $P < 0.05$, sample size $n = 10$) were used to determine differences between the cultivars.
Different lower case letters in a column indicate significant differences.
UGA, unidentified glycoalkaloid.

Table 3 Composition of sugar and its derivatives in tomato fruits of the mutant and three cultivars

Metabolite	Method	Arbitrary unit (AU) ±SD			
		Ec-1	RC17	K091	KGM942
Sugars					
***N*-Acetyl-glucosamine**	GC	26.41 ± 0.27a	26.61 ± 0.43a	26.76 ± 0.40a	27.69 ± 0.73b
1,6-Anhydro-β-glucose	GC	7.97 ± 3.04a	8.65 ± 2.94a	10.34 ± 1.85a	8.01 ± 2.32a
Arabinose	GC	30.90 ± 0.17b	29.40 ± 0.49a	29.82 ± 0.59a	34.03 ± 0.47c
Fructose	GC	37.14 ± 1.96a	37.99 ± 1.13a	40.01 ± 0.71b	39.82 ± 1.19b
Fructose-6-phosphate	GC	22.91 ± 0.22b	22.45 ± 0.22a	22.19 ± 0.25a	22.41 ± 0.18a
Glucose	GC	37.22 ± 0.06a	37.33 ± 0.07b	37.43 ± 0.06c	37.31 ± 0.06b
Glucose-6-phosphate	GC	30.89 ± 0.23a	31.48 ± 0.28b	31.34 ± 0.30b	30.83 ± 0.31a
Galactose	GC	29.43 ± 0.16c	27.43 ± 0.42ab	27.22 ± 0.40a	27.82 ± 0.39b
Maltose	GC	21.21 ± 0.24a	22.12 ± 0.17b	22.64 ± 0.28c	22.37 ± 0.28bc
Raffinose	GC	18.69 ± 1.20a	17.72 ± 1.20a	18.04 ± 1.76a	18.87 ± 1.09a
Ribose	GC	35.55 ± 0.64c	34.48 ± 0.50b	32.71 ± 0.53a	34.36 ± 0.6b
Sucrose	GC	28.99 ± 0.51a	29.40 ± 0.27a	30.25 ± 0.35b	30.25 ± 0.33b
Trehalose	GC	28.81 ± 0.61a	30.47 ± 0.42bc	30.98 ± 0.36c	30.34 ± 0.52b
Xylose	GC	33.71 ± 0.24a	33.87 ± 0.26a	33.70 ± 0.29a	35.04 ± 0.28b
Sugar acids					
Galacturonic acid	GC	36.72 ± 0.92b	35.45 ± 0.77a	35.94 ± 0.38ab	38.19 ± 0.32c
Gluconic acid	GC	25.99 ± 0.75b	25.09 ± 1.05ab	22.15 ± 5.04a	23.89 ± 2.81ab
Glucuronic acid-e-lactone	GC	30.46 ± 0.51b	29.75 ± 0.44a	30.11 ± 0.28ab	31.39 ± 0.23c
Glyceric acid	GC	29.53 ± 0.29c	26.67 ± 0.76b	27.45 ± 0.67b	25.10 ± 0.77a
Saccharic acid	GC	26.49 ± 0.54b	25.71 ± 0.90a	25.54 ± 0.47a	28.89 ± 0.35c
Sugar alcohols					
Galactinol	GC	26.79 ± 0.53a	28.21 ± 0.43b	27.29 ± 0.41ab	28.80 ± 0.35c
Glycerol	GC	27.93 ± 0.24b	27.10 ± 0.19a	26.87 ± 0.37a	27.99 ± 0.23b
myo-Inositol	GC	39.88 ± 0.28c	38.89 ± 0.30b	39.59 ± 0.24c	38.29 ± 0.35a
Sugar phosphate					
Inositol-1-phosphate	GC	23.05 ± 0.18b	22.33 ± 0.30a	22.57 ± 0.36a	23.36 ± 0.24b

All data were log2 transformed. Metabolites in bold are significantly different between the mutant variety KGM942 and the wild-type varieties, Ec-1, RC17 and K091.
All comparisons among means (ANOVA and Tukey's test; $P < 0.05$, sample size $n = 10$) were used to determine differences between the cultivars. Different lower case letters in a column indicate significant differences.

Table 4 Carotenoid composition in tomato fruits of the mutant and threecultivars

Metabolite	Method	Arbitrary unit (AU) ±SD			
		Ec-1	RC17	K091	KGM942
β-Carotene	HPLC	0.16 ± 0.02b	0.18 ± 0.04b	0.13 ± 0.02a	0.11 ± 0.01a
Lycopene	HPLC	0.88 ± 0.09b	0.70 ± 0.13a	0.87 ± 0.12b	1.22 ± 0.12c

The data were quantitative values (mg g^{-1} DW). The metabolite in bold is significantly different between the mutant variety KGM942 and the wild-type varieties, Ec-1, RC17 and K091.
All comparisons among means (ANOVA and Tukey's test; $P < 0.05$, sample size $n = 10$) were used to determine differences between the cultivars. Different lower case letters in a column indicate significant differences.

suppression lines to reproduce the *pe lg* phenotype in the wild-type background (**Fig. 2**). The water permeability of the leaves and fruit was elevated in the *CD2* suppression lines (**Figs. 4**, **7**). An increase in water permeability was also previously reported in the fruit and leaves of the *pe lg* mutant (Isaacson et al. 2009, Kimbara et al. 2012, Nadakuduti et al. 2012). As the suppression lines had slightly fewer stomata than the wild type (**Supplementary Fig. S3**), it is clear that cuticular transpiration is enhanced in these lines. Thus, water use efficiency was lower in the suppression lines, as in the *pe lg* mutant (**Fig. 5c**). However, Chl *a* content and photosynthetic ability were not significantly different between the suppression lines and Micro-Tom (**Fig. 5a**; **Supplementary Fig. S2**), even though the suppression lines showed enhanced transpiration. The water

supply to the roots may be sufficient to drive transpiration in the aerial parts, because of the limited leaf number of Micro-Tom (**Fig. 2c**).

The young leaves of the suppression lines were light green (**Fig. 2b**). This is consistent with the *lg* phenotype, which is possibly due to a lack of anthocyanin (Nadakuduti et al. 2012). As reported in a previous study (Kimbara et al. 2012), a thin, pale cuticle layer on the adaxial side was observed in the suppression lines (**Fig. 3**), suggesting that *CD2* suppression affects proper cuticle formation in the leaf. We currently cannot explain why the cuticle of the abaxial side is not altered in the suppression lines. Further studies are needed to clarify the differences in leaf cuticle structure and composition between the adaxial and abaxial leaf surfaces of the suppression lines. Additionally, mutation or suppression of *CD2* resulted in enhanced external water penetration into the fruit (**Fig. 7b**; Kimbara et al. 2012), while the rate of internal water transpiration is probably not as great as that of external water penetration (**Fig. 7a**). These results imply that the water permeability resulting from *CD2* inhibition may vary in different tissues. Future studies are required to clarify the effect of CD2 on the structural and physiological properties of the cuticle and to establish its role during cuticle formation.

Mutation of *CD2* might partially alter fruit metabolite levels

Histological and physiological observations revealed that drastic alterations occur in the cuticle of the *cd2* mutant. Previous studies showed that the amount and composition of cutin and wax are greatly and slightly altered, respectively, in the *cd2* mutant (Isaacson et al. 2009, Nadakuduti et al. 2012). This suggests that the levels of other lipidic metabolites may also be altered in the mutant. To test this possibility, we performed metabolite profiling analyses on three wild-type varieties and the *cd2* mutant. We observed notable differences, particularly in lipid- and sugar-related metabolites, between the wild type and the *cd2* mutant.

Increases in most galactolipids (**Table 1**) indicate that lipid metabolic pathways in the *cd2* mutant might be affected by the thinner cuticle, as lipidic compounds are loaded into this structure. Consistent with this hypothesis, increases in some phospholipids were observed (**Table 1**). Alternatively, these increases in galactolipids could be caused by changes in sugar metabolism. In accordance with this idea, sugar and the sugar-related metabolites, arabinose, xylose, glucuronic acid-e-lactone, saccharic acid, galactinol, and galacturonic acid, which is a major component of pectin, are more abundant in *cd2*, suggesting that sugar-related metabolic pathways may also be affected in this mutant (**Table 3**). Stakhova et al. (2001) pointed out that an increased concentration of quercetin affected the amount and composition of sugars in tomato fruits, indicating that increases in several flavonoids in the *cd2* mutant may alter some sugar components. However, this seems unlikely, because the major sugar components of tomato fruit, such as glucose, fructose and their derivatives, are not significantly different between the wild-type varieties and the *cd2* mutant (**Table 3**).

As described above, flavonoids, such as kaempferol-3-*O*-rutinoside, naringenin dihexose, quercetin-dihexose-deoxyhexose and rutin, are more abundant in the mutant (**Table 2**). This may be attributed to a change in lipid metabolites of the mutant, because flavonoids are synthesized from malonyl-CoA, which is a precursor of fatty acids. Furthermore, differences in the cuticle structure itself may affect flavonoid composition. Compared with wild-type varieties, the concentration of kaempferol-3-*O*-rutinoside, naringenin dihexose, quercetin-dihexose-deoxyhexose and rutin, which are downstream metabolites in the flavonoid biosynthetic pathways (Slimestad et al. 2009), were dramatically increased in the mutant (**Table 2**). Generally, the main flavonoid in tomato peel is naringenin chalcone, while the tomato pericarp contains a limited amount of rutin (Muir et al. 2001, Bovy et al. 2002, Verhoeyen et al. 2002). However, the naringenin content in the peel of the *pe lg* mutant is lower than that of wild-type varieties (Kimbara et al. 2012). It is possible that the mutant peel is too thin to accumulate sufficient amounts of naringenin chalcone, which promotes the synthesis of downstream metabolites in the flavonoid/flavonol pathways. Alternatively, the *cd2* mutation might alter gene expression to promote flavonoid biosynthesis. In support of this latter hypothesis, CD2 is a transcription factor and ANL2, which is an ortholog of CD2, affects anthocyanin accumulation in the leaf (Kubo et al. 1999). Further studies are needed to determine when and where flavonoids accumulate in the mutant fruit.

Glycoalkaloids such as tomatine and escleoside are abundant in the mutant (**Table 2**). Similar to several flavonoid compounds, glycoalkaloids are also glycosylated, suggesting that changes in sugar metabolism may underlie the mutant phenotype. However, we do not know why glycoalkaloid accumulates in the mutant. A recent study established that glycoalkaloids preferentially accumulate in the peel of tomato (Mintz-Oron et al. 2008). Thus, the increase in glycoalkaloid content may reflect structural changes in the mutant cuticle.

In this study, we have revealed that mutation or reduction of *CD2* has pleiotropic effects. Consistent with previous reports (Isaacson et al. 2009, Kimbara et al. 2012, Nadakuduti et al. 2012), an abnormal cuticle in the mutant causes physiological alterations in both the vegetative and reproductive tissues. In addition, metabolite profiling suggests that lipid and sugar pathways might be altered in the *cd2* mutant. Further studies should clarify the relationship between a thinner cuticle and metabolite changes detected in the fruit.

Materials and Methods

Plant materials

To identify the locus underlying the *pe lg* mutation, F_2 mapping populations were created between *Solanum lycopersicum* cv. KGM942 carrying the *pe lg* mutations (*pe*/*pe*, *lg*/*lg*) and a

wild-type variety Rejina (*PE/PE*, *LG/LG*; Sakata Seeds), and an introgression line IL1-2, which carries the chromosomal segment of *S. pennellii* from the centromeric region to TG295 (92.7 cM) of chromosome 1. IL1-2 was obtained from the University of Tsukuba, Gene Research Center, through the National Bio-Resource Project (NBRP) of the Ministry of Education, Culture, Sports, Science and Technology in Japan (MEXT), Japan. For metabolomic analysis, we used KGM942 and three other wild-type breeding lines (Ec-1, RC17 and K091). The physiological characteristics of these three varieties have previously been shown to be similar (Kimbara et al. 2012).

Fine mapping of the *PE LG* gene

A previous report showed that *PE LG* is located on chromosome 1 (Kerr 1982). To map the location of the *PE LG* gene, 334 F_2 plants derived from a cross between KGM942 and Rejina were genotyped with three markers (C2_At2g38730, C2_At3g04710 and SSR222) on chromosome 1 (**Supplementary Table S1**). For fine mapping of *PE LG*, 336 F_2 plants derived from a cross between KGM942 and IL1-2 were genotyped for 12 markers around the introgression of chromosome 1. All markers used in the fine mapping are described in **Supplementary Table S2**.

Vector construction for down-regulation of *CD2*

To create an antisense construct targeted for *CD2* suppression, a cDNA clone (LEFL2020A13, obtained from NBRP) was used to amplify the full-length coding region of *CD2* using two gene-specific primers, CD2AS-F, 5′-TTTGAGCTCATGAATTTTGGG GGTTTTCT-3′ and CD2AS-R, 5′-TTTGGATCCTTAGCTTTCG CATTGAAGTG-3′. The amplified fragment was digested with *Bam*HI and *Sac*I, and the resulting fragment was purified using MiniElute (QIAGEN). The pBI121 binary vector was also digested with *Bam*HI and *Sac*I, and dephosphorylated with Antarctic Phosphatase (New England BioLabs). The treated vector was purified using the QIAEXII Gel Extraction Kit (QIAGEN). The purified PCR fragment was ligated into dephosphorylated pBI121 vector using a DNA Ligation Kit LONG (TAKARA BIO INC.), and the resulting construct was designated *pBI-CD2-AS*.

The *pBI-CD2-AS* construct was then transformed into *Agrobacterium tumefaciens* GV2205 by the freeze–thaw method (An et al. 1988). The construct was expressed in Micro-Tom by *Agrobacterium*-mediated transformation (Sun et al. 2006). The transgenic plants were selected on Murashige and Skoog (MS) agar medium containing 100 mg l^{-1} kanamycin. Diploid transgenic lines were selected using a cytofluorometer, and T_0 or T_1 generations were used for further studies.

Gene expression analysis

CD2 expression was analyzed by reverse transcription–PCR (RT–PCR) using total RNA extracted from the roots, leaves, flowers, green fruits and red fruits using the RNeasy Plant Mini Kit (QIAGEN). cDNA was synthesized from 1 μg of total RNA using the ReverTra Ace qPCR RT Kit (TOYOBO). The RT–PCR experiment was performed using KOD FX with the following conditions: 2 min of denaturation at 94°C, followed by 30 cycles of 10 s of denaturation at 98°C, 30 s of annealing at 59°C and 1 min of extension at 68°C. As a control, *ACTIN* was amplified using the gene-specific primers Tom52F2, 5′-CCTAG TATTGTGGGACGTCC-3′ and Tom52R, 5′-TAGATCCTCCGAT CCAGACA-3′. The following primers were used to amplify *CD2* mRNA: CD2_1928F, 5′-TCTGGGCTGTCGTTGATGTA-3′ and CD2_4775R, 5′-CCATTACATGAAGGCCCATT-3′. To determine the level of *CD2* suppression in transgenic lines, the gene-specific primers CD2-106F, 5′-GGATTCGTCCTTGTGTC TCCTCTACCTCTC-3′ and CD2_743R, 5′-CCTTCATCTGAGTT CTACGATTTTG-3′ were used. The levels of mRNA accumulation were semi-quantified by measuring the corresponding electrogram peaks using the QIAXcel system (QIAGEN).

Measurement of Chl contents

Chl content was measured as described by Porra et al. (1989). Five excised pieces of mature leaf (100–200 mg FW) of different plants grown in a greenhouse were collected. The leaf pieces were immersed overnight in 3 ml of *N*,*N*-dimethylformamide at 4°C. The concentration of total Chl was calculated in the fresh leaf tissue, as follows: total micrograms of Chl *a* per gram = $12.00\times(A_{664}) - 3.11\times(A_{647})$; total micrograms of Chl *b* per gram = $20.78\times(A_{647}) - 4.88\times(A_{664})$.

Evaluation of water permeability of leaves

To evaluate the water permeability of leaves, the transpiration rate was measured (Kimbara et al. 2012) and the TB test was performed. Prior to sampling, the plants were treated with 500 mg l^{-1} ABA to ensure stomatal closure. Five mature leaves were collected and incubated in constant darkness at 25°C. The fresh weights of the leaves were measured after 0, 1, 2 and 3 h of incubation. The TB test was conducted as described by Tanaka et al. (2004). Briefly, the leaves were immersed in 0.05% TB solution for 1 h. Because tomato leaves are highly hydrophobic, 0.05% NP-40 was added to the TB solution.

Evaluation of water permeability of fruits

The water permeability of the fruits was evaluated based on the transpiration rate and the results of the TB test. To determine the transpiration rate, the fresh weight of the fruit was measured at 0, 1, 2, 3 and 4 d after incubation at 40°C. The TB test was conducted using mature green fruits. The fruits were immersed in 0.05% TB solution with 0.05% NP-40 for 1 h.

Histological observations

The cuticle layer of fruits was observed after the surface lipids were stained with Sudan IV, as described by Buda et al. (2009). TEM was conducted as described previously (Kimbara et al. 2012).

Photosynthetic rate measurement

The youngest fully expanded leaf was used to measure the photosynthetic rate using an open gas exchange system

(Li-6400XT, Li-Cor, Inc.). The net photosynthetic rate (A), stomatal conductance (g_s) and transpiration rate (E) were measured between 09:00 h and 12:00 h at 0, 50, 100, 200, 500, 1,000 and 1,500 μmol m^{-2} s^{-1} PPFD. During the measurements, the relative humidity was maintained at 70%, the CO_2 concentration at 350 p.p.m. and leaf temperature at 28 ± 0.5°C in the leaf chamber. Water use efficiency was calculated as A/E, where A represents the photosynthesis rate and E represents the transpiration rate. T_1 lines of AS38 were used as a suppression line.

Measurement of stomatal density

Mature leaves were observed under a scanning electron microscope (300X, TM-1000, Hitachi High-technologies) without fixation and coating, according to the manufacturer's protocols. Images of 0.36 mm^2 leaf areas were taken from five distinct leaves from both the adaxial and abaxial surfaces of Micro-Tom and AS38.

Metabolite profiling

Meta data from metabolomics studies, formatted according to the guidelines of The Metabolomics Standards Initiative, are given in **Supplementary text S1**.

Statistical analyses

All comparisons among means [analysis of variance (ANOVA) and Tukey's test; $P < 0.05$] were used to determine statistically significant differences between the samples. Data are presented as means and SD with a level of significance of 5% ($P = 0.05$).

Supplementary data

Supplementary data are available at PCP online.

Funding

The work was supported by the Program for Promotion of Basic and Applied Researches for Innovations in the Bio-oriented Technology Research Advancement Institution (BRAIN) of Japan [grant No. ADA23108]; the Japan Advanced Plant Science Network; the RIKEN Plant Transformation Network [the production of transgenic plants].

Acknowledgments

We thank Mr. Makoto Kobayashi (RIKEN CSRS, Japan) for sample preparation for the metabolite profiling analyses and metabolite profiling analyses using GC-TOF-MS and LC-qTOF-MS instruments. We also thank Mr. Makoto Suzuki and Mr. Koji Takano for metabolite profiling analyses using GC-TOF-MS and LC-q-TOF-MS instruments (RIKEN CSRS, Japan). We are grateful to Dr. Arnaud Bovy (Plant Breeding, Wageningen UR, Wageningen, The Netherlands) for helpful advice and discussions.

Disclosures

The authors have no conflicts of interest to declare.

References

Aarts, M.G., Keijzer, C.J., Stiekema, W.J. and Pereira, A. (1995) Molecular characterization of the *CER1* gene of *Arabidopsis* involved in epicuticular wax biosynthesis and pollen fertility. *Plant Cell* 7: 2115–2127.

An, G., Ebert, R., Mitra, A. and Ha, S. (1988) Binary vectors. *In* Plant Molecular Biology Manual. Edited by Gelvin, S.B. and Schilpeoort, R.A. pp. 1–19. Kluwer, Dordrecht, The Netherlands.

Bargel, H. and Neinhuis, C. (2005) Tomato (*Lycopersicon esculentum* Mill.) fruit growth and ripening as related to the biomechanical properties of fruit skin and isolated cuticle. *J. Exp. Bot.* 56: 1049–1060.

Bessire, M., Chassot, C., Jacquat, A.C., Humphry, M., Borel, S., Petétot, J.M.D.C. et al. (2007) A permeable cuticle in *Arabidopsis* leads to a strong resistance to *Botrytis cinerea*. *EMBO J.* 26: 2158–2168.

Bovy, A., de Vos, R., Kemper, M., Schijlen, E., Pertejo, M.A., Muir, S. et al. (2002) High-flavonol tomatoes resulting from the heterologous expression of the maize transcription factor genes LC and C1. *Plant Cell* 14: 2509–2526.

Buda, G.J., Isaacson, T., Matas, A.J., Paolillo, D.J. and Rose, J.K.C. (2009) Three-dimensional imaging of plant cuticle architecture using confocal scanning laser microscopy. *Plant J.* 60: 378–385.

Butler, L. (1952) *Sticky peel* (*pe*), a new character in the seventh linkage group. *TGC Report* 2: 2–3.

Curvers, K., Seifi, H., Mouille, G., de Rycke, R., Asselbergh, B., Hecke, A.V. et al. (2010) Abscisic acid deficiency causes changes in cuticle permeability and pectin composition that influence tomato resistance to *Botrytis cinerea*. *Plant Physiol.* 154: 847–860.

Heredia, A. (2003) Biophysical and biochemical characteristics of cutin, a plant barrier biopolymer. *Biochim. Biophys. Acta* 1620: 1–7.

Hovav, R., Chehanovsky, N., Moy, M., Jetter, R. and Schaffer, A.A. (2007) The identification of a gene (*Cwp1*), silenced during Solanum evolution, which causes cuticle microfissuring and dehydration when expressed in tomato fruit. *Plant J.* 52: 627–639.

Isaacson, T., Kosma, D.K., Matas, A.J., Buda, G.J., He, Y., Yu, B. et al. (2009) Cutin deficiency in the tomato fruit cuticle consistently affects resistance to microbial infection and biomechanical properties, but not transpirational water loss. *Plant J.* 60: 363–377.

Jetter, R. and Kunst, L. (2008) Plant surface lipid biosynthetic pathways and their utility for metabolic engineering of waxes and hydrocarbon biofuels. *Plant J.* 54: 670–683.

Jetter, R., Schäffer, S. and Riederer, M. (2001) Leaf cuticular waxes are arranged in chemically and mechanically distinct layers: evidence from Prunus laurocerasus L. *Plant Cell Environ.* 23: 619–628.

Kerr, E. (1982) New residents on chromosome 1: *rvt*, *vi*, *lg*, *pe*, *dp*, *Nr-2*, *tmf*, *cjf*. *TGC Report* 32: 16–17.

Kimbara, J., Yoshida, M., Ito, H., Hosoi, K., Kusano, M., Kobayashi, M. et al. (2012) A novel class of *sticky peel* and *light green* mutations causes cuticle deficiency in leaves and fruits of tomato (*Solanum lycopersicum*). *Planta* 236: 1559–1570.

Kosma, D.K., Bourdenx, B., Bernard, A., Parsons, E.P., Lü, S., Joubès, J. et al. (2009) The impact of water deficiency on leaf cuticle lipids of *Arabidopsis*. *Plant Physiol.* 151: 1918–1929.

Kubo, H. and Hayashi, K. (2011) Characterization of root cells of *anl2* mutant in *Arabidopsis thaliana*. *Plant Sci.* 180: 679–685.

Kubo, H., Peeters, A.J.M., Aarts, M.G.M., Pereira, A. and Koornneef, M. (1999) *ANTHOCYANINLESS2*, a homeobox gene affecting anthocyanin distribution and root development in Arabidopsis. *Plant Cell* 11: 1217–1226.

Kunst, L. and Samuels, A. (2003) Biosynthesis and secretion of plant cuticular wax. *Prog. Lipid Res.* 42: 51–80.

Leide, J., Hildebrandt, U., Vogg, G. and Riederer, M. (2011) The *positional sterile* (*ps*) mutation affects cuticular transpiration and wax biosynthesis of tomato fruits. *J. Plant Physiol.* 168: 871–877.

Li, Y. and Beisson, F. (2009) The biosynthesis of cutin and suberin as an alternative source of enzymes for the production of bio-based chemicals and materials. *Biochimie* 91: 685–691.

Li, Y., Beisson, F., Koo, A.J.K., Molina, I., Pollard, M. and Ohlrogge, J. (2007) Identification of acyltransferases required for cutin biosynthesis and production of cutin with suberin-like monomers. *Proc. Natl Acad. Sci. USA* 104: 18339–18344.

Lolle, S.J., Hsu, W. and Pruitt, R.E. (1998) Genetic analysis of organ fusion in *Arabidopsis thaliana*. *Genetics* 149: 607–619.

Millar, A.A., Clemens, S., Zachgo, S., Giblin, E.M., Taylor, D.C. and Kunst, L. (1999) *CUT1*, an *Arabidopsis* gene required for cuticular wax biosynthesis and pollen fertility, encodes a very-long-chain fatty acid condensing enzyme. *Plant Cell* 11: 825–838.

Mintz-Oron, S., Mandel, T., Rogachev, I., Feldberg, L., Lotan, O., Yativ, M. et al. (2008) Gene expression and metabolism in tomato fruit surface tissues. *Plant Physiol.* 147: 823–851.

Muir, S.R., Collins, G.J., Robinson, S., Hughes, S., Bovy, A., Ric De Vos, C.H. et al. (2001) Overexpression of petunia chalcone isomerase in tomato results in fruit containing increased levels of flavonols. *Nat. Biotechnol* 19: 470–474.

Nadakuduti, S.S., Pollard, M., Kosma, D.K., Allen, C., Ohlrogge, J.B. and Barry, C.S. (2012) Pleiotropic phenotypes of the *sticky peel* mutant provide new insight into the role of *CUTIN DEFICIENT2* in epidermal cell function in tomato. *Plant Physiol.* 159: 945–960.

Panikashvili, D., Savaldi-Goldstein, S., Mandel, T., Yifhar, T., Franke, R.B., Höfer, R. et al. (2007) The *Arabidopsis DESPERADO/AtWBC11* transporter is required for cutin and wax secretion. *Plant Physiol.* 145: 1345–1360.

Pollard, M., Beisson, F., Li, Y. and Ohlrogge, J.B. (2008) Building lipid barriers: biosynthesis of cutin and suberin. *Trends Plant Sci.* 13: 236–246.

Porra, R.J., Thompson, W.A. and Kriedemann, P.E. (1989) Determination of accurate extinction coefficients and simultaneous equations for assaying chlorophylls a and b extracted with four different solvents: verification of the concentration of chlorophyll standards by atomic absorption spectroscopy. *Biochim. Biophys. Acta* 975: 384–394.

Riederer, M. (2007) Introduction: biology of the plant cuticle. *In* Biology of the Plant Cuticle. Edited by Riederer, M. and Müller, C. pp. 1–10. Blackwell, Oxford.

Samuels, L., Kunst, L. and Jetter, R. (2008) Sealing plant surfaces: cuticular wax formation by epidermal cells. *Annu. Rev. Plant Biol.* 59: 683–707.

Schnurr, J., Shockey, J. and Browse, J. (2004) The acyl-CoA synthetase encoded by *LACS2* is essential for normal cuticle development in Arabidopsis. *Plant Cell* 16: 629–642.

Slimestad, R. and Verheul, M. (2009) Review of flavonoids and other phenolics from fruits of different tomato (*Lycopersicon esculentum* Mill.) cultivars. *J. Sci. Food Agric.* 89: 1255–1270.

Stakhova, L.N., Ladygin, V.G. and Stakhov, L.F. (2001) The effect of quercetin on the accumulation of carbohydrates and amino acids in tomato fruits. *Russ. J. Plant Physiol.* 48: 191–195.

Sun, H.-J., Uchii, S., Watanabe, S. and Ezura, H. (2006) A highly efficient transformation protocol for Micro-Tom, a model cultivar for tomato functional genomics. *Plant Cell Physiol.* 47: 426–431.

Tanaka, T., Tanaka, H., Machida, C., Watanabe, M. and Machida, Y. (2004) A new method for rapid visualization of defects in leaf cuticle reveals five intrinsic patterns of surface defects in Arabidopsis. *Plant J.* 37: 139–146.

Verhoeyen, M.E., Bovy, A., Collins, G., Muir, S., Robinson, S., de Vos, C.H.R. et al. (2002) Increasing antioxidant levels in tomatoes through modification of the flavonoid biosynthetic pathway. *J. Exp. Bot.* 53: 2099–2106.

Vogg, G., Fischer, S., Leide, J., Emmanuel, E., Jetter, R., Levy, A.A. et al. (2004) Tomato fruit cuticular waxes and their effects on transpiration barrier properties: functional characterization of a mutant deficient in a very-long-chain fatty acid beta-ketoacyl-CoA synthase. *J. Exp. Bot.* 55: 1401–1410.

Xiao, F., Goodwin, S.M., Xiao, Y., Sun, Z., Baker, D., Tang, X. et al. (2004) Arabidopsis *CYP86A2* represses *Pseudomonas syringae* type III genes and is required for cuticle development. *EMBO J.* 23: 2903–2913.

Yeats, T.H., Martin, L.B.B., Viart, H.M.F., Isaacson, T., He, Y., Zhao, L. et al. (2012) The identification of cutin synthase: formation of the plant polyester cutin. *Nat. Chem. Biol.* 8: 609–611.

Yephremov, A. and Schreiber, L. (2005) The dark side of the cell wall: molecular genetics of plant cuticle. *Plant Biosyst.* 139: 74–79.

Zou, L., Sun, X., Zhang, Z., Liu, P., Wu, J., Tian, C. et al. (2011) Leaf rolling controlled by the homeodomain leucine zipper class IV gene *Roc5* in rice. *Plant Physiol.* 156: 1589–1602.